An AMR Sensor-Based Measurement System for Magnetoelectrical Resistivity Tomography

Egon Zimmermann, Arre Verweerd, Walter Glaas, Axel Tillmann, and Andreas Kemna

***Abstract*—A magnetoelectrical resistivity measurement system is proposed, which combines measurement of the electric potential and the magnetic field due to a current injection into a sample. Measurement of the electric potential, as well as the injected current, is similar to traditional electrical resistivity tomography (ERT) data acquisition. For the magnetic field measurements, 24 sensor modules have been developed using three component anisotropic magnetoresistive (AMR) sensors, mounted on a vertically moving scanning torus. The system is designed to operate in a typical laboratory magnetic noise environment without extensive shielding. To compensate for the effects of the Earth's magnetic field, the AMR sensors are operated with a field feedback circuit. Optimal noise reduction is provided by the use of a lock-in frequency of 25 Hz, with sine wave modulation and measurement cycles of 10 s. The resolution of the system is better then 50 pT and the aimed accuracy is 0.1%. The system provides a data set of magnetic fields complimentary to traditional ERT to determine the internal conductivity distribution of cylindrical samples with the dimension of 0.1-m radius and 0.5-m height.**

***Index Terms*—Anisotropic magnetoresistive (AMR), electrical resistivity tomography (ERT), magnetic sensors, magnetometric resistivity (MMR).**

I. Introduction

THE Maxwell equations reflect the close relationship between the electrical conductivity and respectively electrical and magnetic fields due to a low frequency current injection into a medium. Measuring both fields can provide information on the internal electrical conductivity distribution of the medium. Therefore, the magnetoelectrical resistivity imaging technique (MERIT) was proposed (see [1] and [2]), which expands traditional electrical resistivity tomography (ERT) with the additional measurement of the magnetic field components.

Main applications for MERIT were suggested to be in the field of hydrogeophysics, where it can be used as an imaging technique for flow and transport processes in soils and sediments [3]. Since MERIT is a noninvasive measurement technique other applications can be in the field of medicine (see [4]) or in industrial problems, imaging of flow through pipes or mixing vessels for instance. Here, we present a data acquisition system for MERIT with a focus on the magnetic field measurements.

II. Theoretical Background

In geophysics, the use of magnetic fields to measure electrical conductivity distributions in the subsurface goes back to the so-called magnetometric (MMR) resistivity method (see [5]). The governing equations of this method can be derived from common magnetostatic relationships.

For a quasistatic point-source current injection I at the origin into a medium, the Poisson equation defines the resulting electric potential in the medium

$$\nabla \cdot [\sigma(r)\nabla V(r)] = -I\delta(r) \tag{1}$$

in which σ denotes the electrical conductivity distribution, V the electric potential, and δ the Dirac delta function. The current flow in the considered volume (with a current density $J(r) = -\sigma(r)\nabla V(r)$) generates a magnetic field according to the law of Biot-Savart, which after application of Stokes' theorem, can be written as

$$B(r) = \frac{\mu}{4\pi} \int_V \frac{\nabla' V(r') \times \nabla \sigma(r')}{|r - r'|} dv' \tag{2}$$

where B is the magnetic flux density, and μ the magnetic permeability, which can be assumed to be $\mu = \mu_0$, the permeability of free space, when magnetization effects are negligible. Equation (2) shows the drawback of the MMR method, no direct measurements of the electrical conductivity are possible, only information on its gradient is contained in the magnetic field. On the other hand, (2) implies that the addition of magnetic field data to a conventional ERT data set can provide complementary information (e.g., [5]). Due to the different sensitivity behavior of MMR measurements, it can be shown that combination of MMR with ERT will increase the resolution of the electrical conductivity imaging [6].

For the reconstruction of the conductivity distribution, the measured sensor voltages u_m are used instead of the magnetic field values. Both are linked by the sensor sensitivity (S_x, S_y, S_z) according to

$$u_m = (S_x,\ S_y,\ S_z) \begin{pmatrix} B_x \\ B_y \\ B_z \end{pmatrix}. \tag{3}$$

Manuscript received January 5, 2004; revised August 9, 2004. The associate editor coordinating the review of this paper and approving it for publication was Dr. Krikor Ozanyan.

E. Zimmermann and W. Glaas are with the Central Institute for Electronics (ZEL), Forschungszentrum Jülich GmbH, Jülich 52425, Germany (e-mail: e.zimmermann@fz-juelich.de; w.glaas@fz-juelich.de).

A. Verweerd is with the Central Institute for Electronics (ZEL), Forschungszentrum Jülich GmbH, Jülich 52425, Germany, and also with the Agrosphere Institute (ICG-IV), Jülich 52425, Germany (e-mail: a.verweerd@fz-juelich.de).

A. Tillmann and A. Kemna are with the Agrosphere Institute, (ICG-IV), Jülich 52425, Germany (e-mail: a.tillmann@fz-juelich.de; a.kemna@fz-juelich.de).

Digital Object Identifier 10.1109/JSEN.2005.843889

For any typical triaxial magnetic sensor, the location of each magnetic axis is different. Therefore, it is difficult to calculate the magnetic field from the sensor voltages at a given sensor position in an inhomogeneous magnetic field.

III. Measurement System Requirements

The MERIT measurement system is designed to operate under magnetic noise conditions which can be found in any typical laboratory. This implies no extensive magnetic shielding system is used in the measurement setup. For the MERIT system, the target accuracy of the measured magnetic field and the geometrical position was fixed at 0.1%.

Typical target dimensions for the MERIT system are cylindrical samples with approximately 0.2-m diameter and 0.5-m height. Our typical measurement scenario involves fluid flow through porous media (e.g., sediments). Due to the dimensions of the cylinder, a relative fast rate of both magnetic field and electrical potential measurements is required. Therefore, the MERIT system is designed as an array based system to accommodate fast scanning of a sample. These conditions impose several requirements which will be discussed in the following sections.

A. Magnetic Field Measurement Range

Traditional field-scale ERT systems in geophysics use currents with a magnitude in the order of several 100 mA. For our system dimensions we assumed a maximum current of 50 mA, which generates at 5-cm distance of a current wire a magnetic field of ± 200 nT. The target measurement accuracy, therefore, was fixed at 200 pT (0.1% of the maximum magnetic field magnitude). The allowed statistical error (σ) should be significantly lower than this value, for instance 50 pT. In this case, more than 99.9% of all measurements fall in the sensor range, when a Gaussian distribution of the measured data is assumed. A low statistical error is also useful for difference measurements to investigate the effect of anomalous objects (see Section VI-B and [7]).

B. Geometrical Accuracy

Since the dimensions of our samples are in the 0.1 m range, the desired accuracy of 0.1% requires a geometrical accuracy of several tenths of a millimeter. The dimensions of the sensor itself also has an effect on the accuracy, influencing the determination of the position of the sensitive magnetic axis for modeling purposes.

C. Measurement Frequency Range and Sensor Noise

The MERIT system is designed to operate in a typical laboratory magnetic noise environment (see Fig. 1). This means the power line interference with its 50-Hz peak due to current flowing in and to electronic appliances has to be taken into account in the choice of the measurement frequency. Induction effects also should be avoided; therefore, our frequency range is limited to below 100 Hz. Measured magnetic noise spectra of our laboratory showed two acceptable frequency ranges: 20 to 40 Hz and 60 to 80 Hz. In these frequency ranges, the magnetic noise is between 10 and 80 $\mathrm{pT}/\sqrt{\mathrm{Hz}}$, which implies that high resolution magnetic field sensors with noise levels lower than 80 $\mathrm{pT}/\sqrt{\mathrm{Hz}}$ are appropriate.

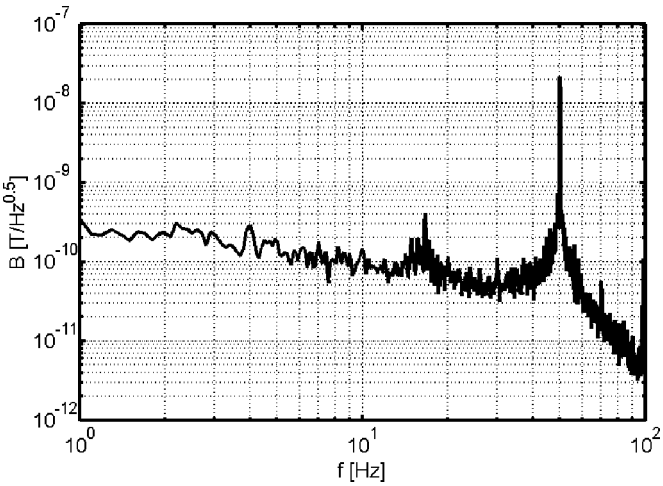

Fig. 1. Typical laboratory noise spectrum measured with a fluxgate sensor (Bartington MAG-03 MSESL).

TABLE I
Theoretical Thermal Noise Level of Investigated Magnetoresistive Sensors

sensor type	thermal noise $\left[\frac{pT}{\sqrt{Hz}}\right]$	type	manufacturer
AA002	46	GMR	NVE
KMZ51	89	AMR	Philips
HMC1023	85	AMR	Honeywell
HMC1001	23	AMR	Honeywell

IV. Sensor Properties and Readout Circuit

Commercially available magnetic sensors show a wide range of sensitivities, geometrical resolution and prices. Superconducting quantum interference device (SQUID) magnetometers are extremely sensitive and have a very good geometrical resolution due to their small size, but they are very expensive and demand a great effort in their operation. Therefore, SQUIDS are not applicable in the planned array based system. Fluxgate magnetometers or induction coils have a good sensitivity but due to their size a rather bad geometrical resolution. Hall sensors have a good geometrical resolution but low sensitivity. Therefore, magnetoresistive (MR) sensors were chosen for this application since they are available as microchips. The sensitivity of MR sensors is not as good as for instance the sensitivity of a fluxgate sensor but because of their small size (several square millimeters) and low price, they are very good candidates for this type of system.

A. Sensor Noise

Several different low noise anisotropic magnetoresistive (AMR) sensors and one giant magnetoresistive (GMR) sensor were investigated (see Table I), each with a theoretical white noise level (thermal noise) lower than 80 $\mathrm{pT}/\sqrt{\mathrm{Hz}}$ when a bridge voltage of 5 V is applied.

In addition to these thermal noise values, a noise spectrum of each sensor was measured (see Fig. 2) in a shielded environment.

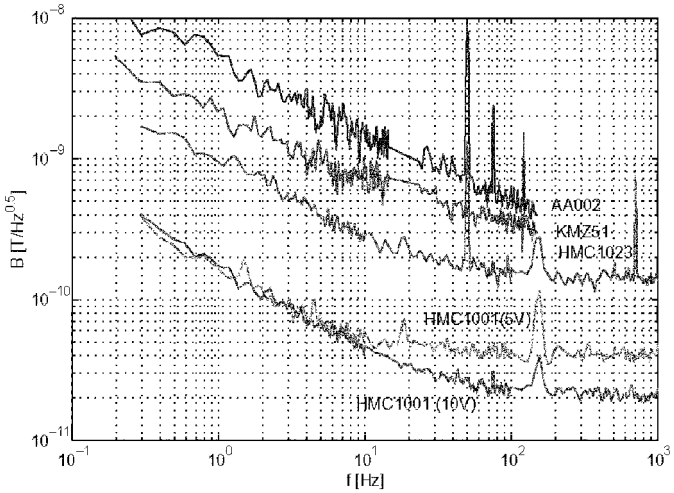

Fig. 2. Noise spectra of different magnetoresistive sensors.

The noise spectrum of the HMC1001 sensor shows the lowest $1/f$ frequency with the thermal noise behavior in the measured frequency range. This implies that when the sensor is operated with a higher bridge voltage of 10 V the noise level is reduced even more. Since the noise spectra of the other sensors are larger than the thermal noise level in the 10–100 Hz frequency range, operation of the sensor with a higher bridge voltage could not reduce the noise level.

Due to the superior noise behavior of the Honeywell HMC1001 AMR sensor with a noise level lower than 50 pT/$\sqrt{\text{Hz}}$ in the 10–100 Hz frequency range, this sensor was chosen for the measurement system.

B. Stability of the Sensor Sensitivity in the Earth's Magnetic Field

An accurate measurement of the magnetic field requires a stable measurement sensitivity of each sensor module. To reach the required accuracy each sensor needs to be calibrated, which is possible only when the measurement sensitivity is independent of any external static magnetic field.

Because the MERIT system is designed to operate in a magnetically nonshielded environment, the effect of the presence and direction of the Earth's magnetic field needs to be negated. The large static Earth's field in comparison with the field range of the sensor has a profound effect on the sensitivity and direction of the sensor's magnetic axis. This effect can be proved by calculation as well as by measurements.

1) Calculated Effect: The sensitivity of a complete single sensor AMR bridge consisting of four Barber-Pole elements (see [8]) can be defined as the variation of its bridge voltage with respect to two directions of the applied magnetic field. When the bridge voltage (U_s) of this circuit is written as a function of the field strength of the sensor's sensitive axis (H_{sen}) and of its orthogonal axis (H_{ort}) (see [9]) it follows that:

$$U_s = U_0 \frac{c\, H_{\text{sen}}}{H_0 + H_{\text{ort}}} \sqrt{1 - \left(\frac{H_{\text{sen}}}{H_0 + H_{\text{ort}}}\right)^2}. \tag{4}$$

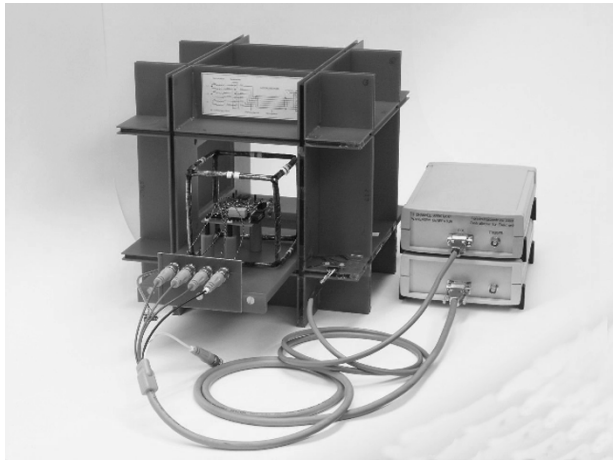

Fig. 3. Sensor sensitivity measurement setup.

The constant H_0 describes the characteristic field strength of the sensor (see [10]), c the AMR sensor's magnetoresistive effect, and U_0 the supply voltage of the bridge. Due to the orientation of the sensor the second orthogonal axis of the sensor (normal to the sensor surface) can be negated and is, therefore, not taken into account.

For small changes in the external ac fields, the sensitivity can then be written as

$$\begin{aligned} S_{\text{ort}} &= \frac{dU_s}{dH_{\text{ort}}} \\ &= -\frac{U_0\, c\, H_{\text{sen}}}{(H_0 + H_{\text{ort}})^2} \sqrt{1 - \left(\frac{H_{\text{sen}}}{H_0 + H_{\text{ort}}}\right)^2} \\ &\quad + \frac{\frac{U_0\, c\, H_{\text{sen}}^3}{(H_0 + H_{\text{ort}})^4}}{\sqrt{1 - \left(\frac{H_{\text{sen}}}{H_0 + H_{\text{ort}}}\right)^2}} \end{aligned} \tag{5}$$

$$\begin{aligned} S_{\text{sen}} &= \frac{dU_s}{dH_{\text{sen}}} \\ &= \frac{U_0\, c}{H_0 + H_{\text{ort}}} \sqrt{1 - \left(\frac{H_{\text{sen}}}{H_0 + H_{\text{ort}}}\right)^2} \\ &\quad - \frac{\frac{U_0\, c\, H_{\text{sen}}^2}{(H_0 + H_{\text{ort}})^3}}{\sqrt{1 - \left(\frac{H_{\text{sen}}}{H_0 + H_{\text{ort}}}\right)^2}} \end{aligned} \tag{6}$$

where S_{ort} and S_{sen} are the sensor sensitivities in its orthogonal and sensitive direction. The relative sensitivities $(S_{\text{ort,sen}}/S_0)$ can then be calculated for static fields with magnitudes similar to the Earth's magnetic field (50 μT). The sensitivity $S_0 = c/H_0$ can be calculated by setting $H_{\text{ort}} = H_{\text{sen}} = 0$.

2) Measured Effect: To measure the sensitivity dependence a triaxial Helmholtz coil was used (see Fig. 3). With the Helmholtz coil, small magnetic fields with an accuracy of 0.1% can be generated. Inside this coil, a second triaxial coil is located, for the generation of the static field. To eliminate the effect of the Earth's magnetic field, both coils are placed inside a magnetically shielded area. Measurements were done for both positive and negative layer magnetization of the sensor $(\pm H_0)$.

TABLE II
SENSOR SENSITIVITY DEPENDENCE ON THE STATIC FIELD. $S_{(ort,sen)t}$ DENOTES CALCULATED VALUES. $S_{(ort,sen)m}$ DENOTES MEASURED VALUES

H_0 $[\frac{A}{m}]$	H_{ort} $[\frac{A}{m}]$	H_{sen} $[\frac{A}{m}]$	$\frac{S_{ortt}}{S_0}$ -	$\frac{S_{ortm}}{S_0}$ -	$\frac{S_{sent}}{S_0}$ -	$\frac{S_{senm}}{S_0}$ -
+637	0.0	0.0	0.000	0.000	1.000	1.000
-637	0.0	0.0	0.000	0.000	1.000	1.000
+637	39.8	0.0	0.000	-0.004	0.941	0.934
-637	39.8	0.0	0.000	+0.005	1.067	1.075
+637	0.0	39.8	-0.062	-0.071	0.994	0.998
-637	0.0	39.8	+0.062	+0.071	0.994	0.994

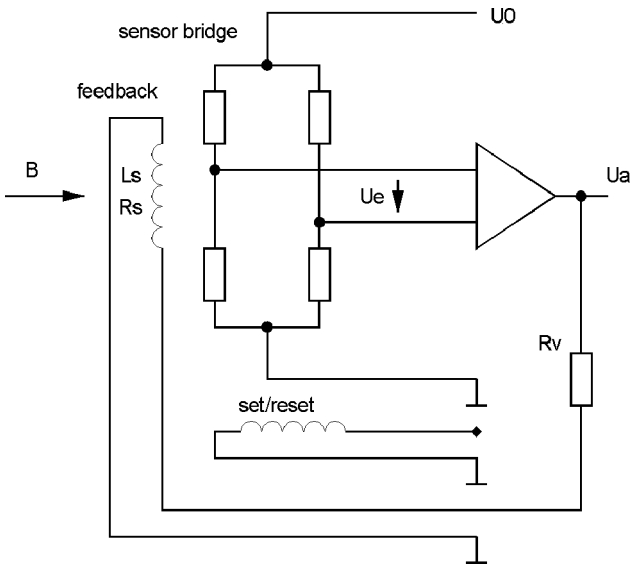

Fig. 4. Field feedback circuit with compensating coil.

The results of both theoretical calculation and measurements (see Table II) show expected measurement errors due to change in sensitivity up to 7%. The influence of static fields affects both directions, thus causing a change in the direction of the magnetic axis of the sensor.

C. Compensation of the Static Field Dependency

Usually, the static field dependency is compensated by means of the so-called flipping technique (see [8]) or the field feedback technique (see [11]). The flipping technique uses the mean values for positive and negative layer magnetization of the sensor. It can be shown, however, that the flipping technique still leaves errors in the sensitivities (see Table II).

Therefore, in order to compensate for the effects of static fields on the sensor sensitivity, a field feedback circuit was implemented (see Fig. 4) instead of the flipping technique. The field feedback circuit uses the integrated compensating coil of the sensor to negate the static field in sensitive direction $(H_{\rm sen})$. Following (5) this causes the sensitivity in the orthogonal axis $S_{\rm ort}$ to be zero at any time.

Using this feedback circuit, the output signal is dependent on the feedback coil sensitivity S_{fb} and no longer on the sensor sensitivity $S_{\rm sen}$. This enables to neglected the dependence on the sensor sensitivity $S_{\rm sen}$. Therefore, the static fields have no effect on the sensitivity S_{fb}.

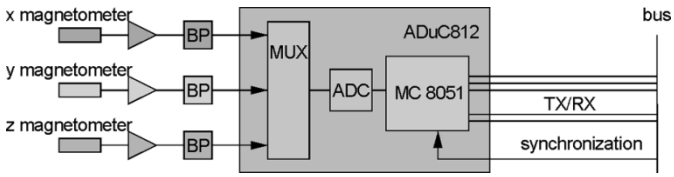

Fig. 5. Block diagram of the MERIT sensor module.

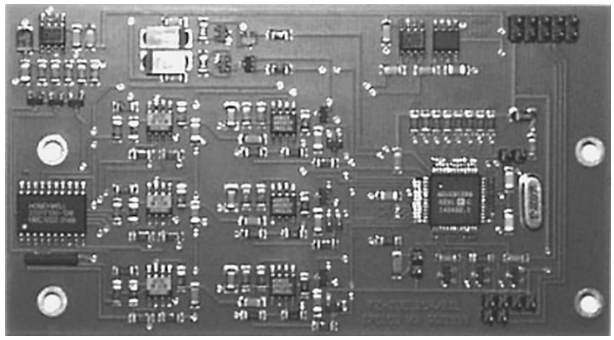

Fig. 6. MERIT sensor module.

Due to the small size of the integrated compensating coils, coupling effects between the three sensors are small. The coupling between the sensors is independent of the static field and is calibrated in the system.

D. Temperature Drift

Since the sensitivity no longer depends on the sensor, but on the feedback coil, temperature drift of the coil and resistor causes errors in the measurements. The magnetic coupling between coil and sensor can be assumed to be temperature independent. Temperature effects in the coil resistance (R_s) and the resistor (R_v) are, therefore, the cause of the drift. After optimization this effect could be limited to 0.1% for a $\pm$5-K temperature change and, therefore, small enough to be neglected.

A drawback of the HMC1001 is the high compensation currents required to compensate the Earth field. Therefore, temperature effects also can be caused by heating in the circuits themselves. Since the compensating currents can be as large as 25 mA, the self heating of the resistor causes a 0.14% error. Implementation of two parallel SMD resistors and a good thermal coupling with the circuit board can dissipate the produced heat adequately.

V. LOCK-IN AMPLIFIER

To implement the three orthogonal sensors into the MERIT measurement system, sensor modules equipped with a lock-in amplifier were designed (see Figs. 5 and 6). Each sensor signal is after amplification and bandpass filtering passed through a multiplexer to an ADC and into a microcontroller (AduC812) were the signals are further processed.

The module design is optimized for low-power consumption and a small amount of electronic circuits to suppress additional magnetic fields due to currents flowing in the module. The module itself is galvanically isolated fixed to the measurement system. All current wires outside the module with currents flowing in the opposite direction are placed close together to

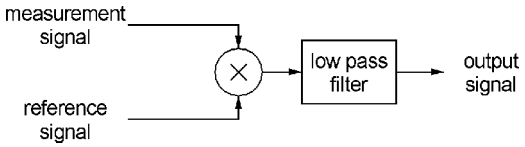

Fig. 7. Schematic signal processing of the lock-in amplifier.

limit the effect of magnetic fields due to the currents flowing through the wires. During the actual measurement, no data communication is necessary with a measuring computer since all necessary processing and data storage is done in the microcontroller, which also limits additional magnetic fields.

A. Phase Sensitive Amplification in MERIT

Improving the signal to noise ratio in the MERIT system, where our target signals are periodical and have a small amplitude, is achieved by the implementation of lock-in techniques.

After the measurement signal $u_m(t)$ is multiplied with a reference signal $(r(t))$, a first-order moving average filter with an integration time of T is applied, functioning as a low pass filter (see Fig. 7). The final output signal (u_{out}), which is passed to the multiplexer, can then be written as

$$u_{\text{out}} = \frac{1}{T}\int_0^T u_m(t)r(t)dt. \tag{7}$$

1) Optimal Reference Signal: Two candidates arise in the choice of the reference signals, a boxcar function and a sine function, each affecting the output signal differently. The use of a sine function as reference limits additional noise when compared to a boxcar reference, which causes the odd harmonics to remain in the signal. When applied to a typical noise measurement of our laboratory, the superior filtering abilities of the sine function reference signal becomes apparent. The output signal calculated with a boxcar reference signal shows a much more noisy spectrum as the sine wave reference output [see Fig. 8(c) and (d)]. Therefore, the sine wave reference was chosen.

2) Optimal Integration Time: The minimal integration time is determined by the white noise of the sensor. The variance σ^2 of the noise is defined as (see [12])

$$\sigma^2 = \int_{\Delta f} B(f)^2 df = B(f)^2 \Delta f_{\text{eq}}. \tag{8}$$

Here, $B(f)$ denotes the noise spectrum of the measured magnetic field [pT/$\sqrt{\text{Hz}}$], Δf denotes the frequency bandwidth, and Δf_{eq} denotes the equivalent noise bandwidth. Transforming (7) to the frequency domain, and applying several calculation steps (see Appendix I) for white noise leads to

$$B(f) = \sigma\sqrt{2T}. \tag{9}$$

The sensor noise value of 50 pT/$\sqrt{\text{Hz}}$, together with the requirement of a standard deviation of 50 pT, leads to a minimal integration time T of 0.5 s.

Unfortunately, simulations of the lock-in amplification with the typical laboratory noise shows higher noise values (see Fig. 8). Simulations with 0.5 s give rise to 100-pT standard deviation or more [see Fig. 8(a)]. An integration time of 3 s should be sufficient to measure with standard deviations of around 50 pT [see Fig. 8(b)]. Most values in the target frequency bandwidth are within this range. Since the dynamics of our measurement targets (flow and transport through porous media) allow a higher measurement cycle time a measurement time of 10 s [see Fig. 8(c)] was chosen. In this case, only a few peaks with amplitudes higher than 50 pT are present.

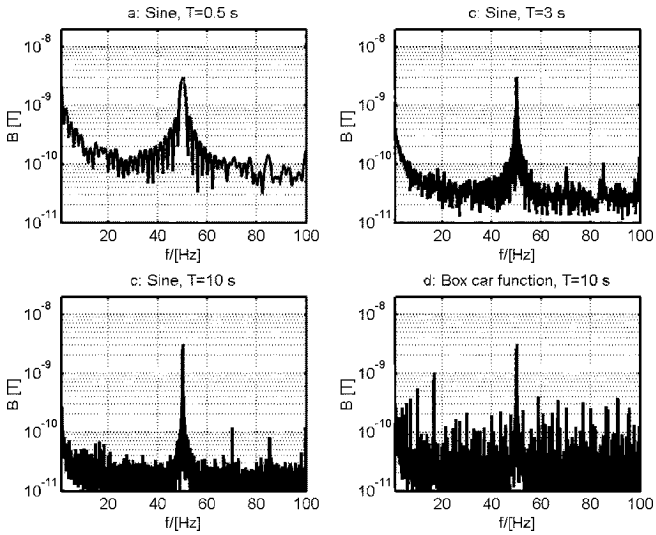

Fig. 8. Effect of different integration times and lock-in frequencies on the noise values of B[T]: (a) 0.5 s; (b) 3 s; (c) 10 s with sine reference signal; (d) 10 s with a boxcar reference signal.

Additional filtering (higher order filters or weighting of the input values) can improve the signal to noise ratio, but were not implemented because of the limited computing power of the used microcontroller.

3) Optimal Lock-In Frequency: As the optimal lock-in frequency 25 Hz was selected. The choice for the 25-Hz frequency was based upon the simulation results in Fig. 8 with different lock-in frequencies in the range from 1 to 100 Hz and provides the lowest noise level between the $1/f$ noise of the sensor and the 50-Hz peak of electrical appliances.

Also, by choosing the low frequency, unwanted induction effect in the sample and its environment could be avoided, when compared to higher frequencies.

4) Synchronization: Because the output signal u_{out} is dependent on the phase between the measurement signal and the reference signal $(u_{\text{out}} \sim \cos\phi)$, the lock-in amplifier needs to be synchronized. The excitation signal and the reference signal in the microcontroller are generated separately. In order to avoid phase errors, the reference signal is synchronized periodically with the sine generator, which generates the injection current. Calculation show measurement errors of less than 100 ppm, and, therefore, can be neglected.

B. ADC Accuracy and Quantization Noise

The measurement modules should be able to measure magnetic fields with an accuracy of 200 pT in the presence of the

Earth's magnetic field with a magnitude of 50 μT. For dc coupling this implicates a measurement range of ± 50 μT and an ADC accuracy of 18 bit. For an AC-coupling the measurement range is ± 200 nT and the required ADC accuracy is only 11 bit, which means a 12 bit ADC with ac-coupling is sufficient for our system.

The quantization noise $(B(f))$ of the ADC should be much lower than the white noise level of the sensor with 50 pT/$\sqrt{\text{Hz}}$. For a one-sided spectrum, the quantization noise can be written as (see [13])

$$B(f) = \sqrt{\frac{Q^2}{6 f_s}}. \tag{10}$$

A quantization step of $Q = 200$ pT and a sampling frequency of $f_s = 1$ kHz leads to a noise of 2.6 pT/$\sqrt{\text{Hz}}$, which clearly is much lower as the white noise level of the sensor.

C. Bandpass Filter

The high pass of the bandpass filter eliminates the dc signal and the $1/f$ noise. The low pass works as an anti-aliasing filter for the ADC. The boundary frequencies of the bandpass filter, where the amplification factor drops to 95% of its maximal value, are 10 and 55 Hz. The center frequency is 23.5 Hz. The phase of the filter decreases almost linearly form $+25°$ to $-25°$ in the frequency range. This phase shift is taken into account in the lock-in amplification.

Unfortunately, the gain and phase are subject to temperature drifts, mainly due to capacities, where changes of 1% due to a 5-K temperature change are common. If this temperature coefficient is assumed to be equal for all capacities, the temperature drift could give rise to changes in the phase of 0.35° in our frequency range, introducing an error of 18 ppm which can be neglected. The amplitude change in the frequency range 10–55 Hz is about 0.13%, and at the center frequency less than 0.05%, introducing a slightly larger error.

VI. Measurement Setup

The design of the scanning system (see Figs. 9 and 10) accommodates the target dimension of our samples. Since MERIT is designed to monitor flow and transport processes on relative small scales, a comparative fast scanning system had to be designed. In addition, the electrical conductivity distribution imaging requires a good spatial sampling. Therefore, a scanning sensor array was designed. A torus with 24 sensor modules at equally spaced distances are lined up at a distance of 0.15 m of the central axis and measure the magnetic field simultaneously. The use of the vertical scanner allows magnetic field measurements at any desired height of the sample. The spatial sampling in the horizontal plane is limited to distance of the modules.

The electrodes used for current injection and measurement of the electrical potential are fixed in the sample (which has a Plexiglas casing) at different heights, and evenly distributed along the surface. A function generator and current amplifier supply the injection current. A measurement PC controls the movement of the vertical belt, the current injection pattern and the potential field measurements. The magnetic data set is send via a BUS to the PC after a single measurement cycle, the electrical potential measurements are directly recorded.

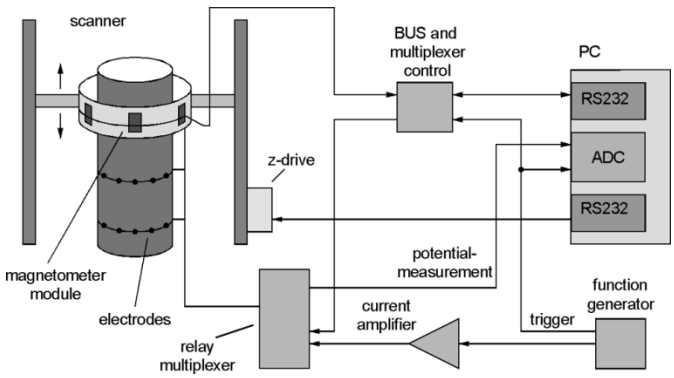

Fig. 9. Block diagram of the MERIT system.

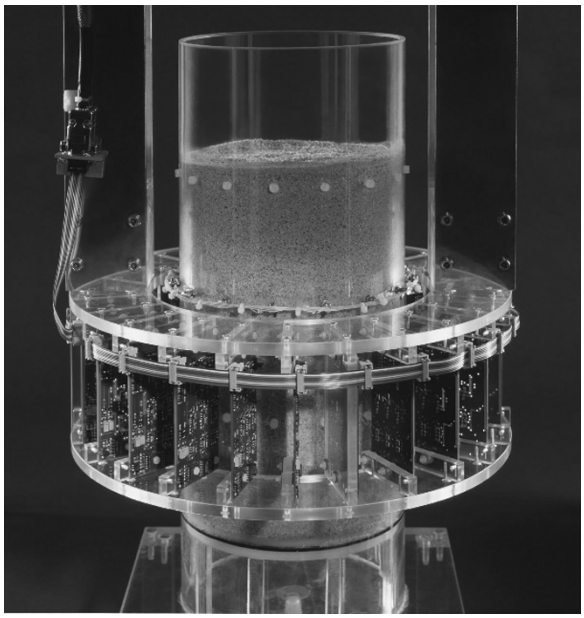

Fig. 10. Photograph of the scanning torus of the MERIT system, including the sensor modules as shown in Fig. 6.

A. Accuracy of the Sensor Axes and Position

The position and the orientation of the sensitive magnetic axis of each AMR sensor with respect to a chosen origin is of great importance. Therefore, the 24 sensor modules are fixed on a solidly build torus with known positions. The accuracy of the vertical moving belt is up to 50 μm.

During fabrication of the modules, a certain error in positioning of the sensors is to be expected. Especially since the module layout uses two AMR chips, one with two AMR sensors and a single AMR sensor. The orientation of the magnetic axis, with the relative sensitivities (S_x/S_r, S_y/S_r, and S_z/S_r) of the AMR chips, in relation to the module circuit board had to be measured (see Table III). The sensitivity S_r in Table III is the absolute value.

The single chip (in the case of the MERIT system the y-axis sensor) shows the largest variation in its orientation, which clearly points to errors in mounting the chip to the circuit board.

TABLE III
ORIENTATION OF THE MAGNETIC AXIS OF THE SENSORS

Sensor	S_x/S_r	S_y/S_r	S_z/S_r
x-sensor	-1.000 ± 0.005	-0.010 ± 0.005	-0.014 ± 0.012
y-sensor	-0.003 ± 0.023	-1.000 ± 0.007	$+0.026 \pm 0.019$
z-sensor	-0.020 ± 0.012	$+0.001 \pm 0.005$	-1.000 ± 0.005

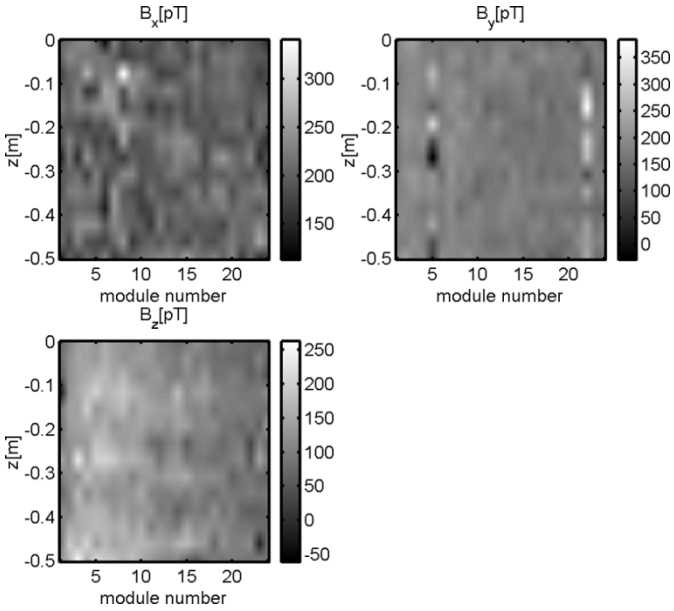

Fig. 11. Test measurements, offset and noise of the magnetic field B_x, B_y, B_z without current injection. The orientation of the magnetic axes x, y, z are in relation to each module circuit board.

In general the error is around 2%, which implies the need for an accurate calibration of the modules.

B. Difference Measurements

Several systematic errors could be suppressed by so-called difference measurements. Each measurement consists of two samples, a homogeneous one and a disturbed one. The measurement configuration is the same and the time interval is short enough to assume that there are no changes in the outside magnetic field. Then, by calculating the difference of both data sets, the effect of current flowing through electric wires and in the circuits is nullified, leaving only the effect of the change in the internal electrical conductivity distribution as a source of the changes in the magnetic signal.

VII. TEST MEASUREMENTS

The first test was to determine offset and noise of the measured magnetic field data of the complete system. At 14 different vertical locations, the magnetic field was measured with the 24 sensor modules in our laboratory, without any current injection in the sample (see Fig. 11).

The mean values of the measured magnetic field for the x and y sensor are 204 and 177 pT, independent of the module and the z position. It points to a constant offset error of 200 pT due to calculation errors in the module. The mean value of the z sensor is 120 pT; however, the z component shows a dependence

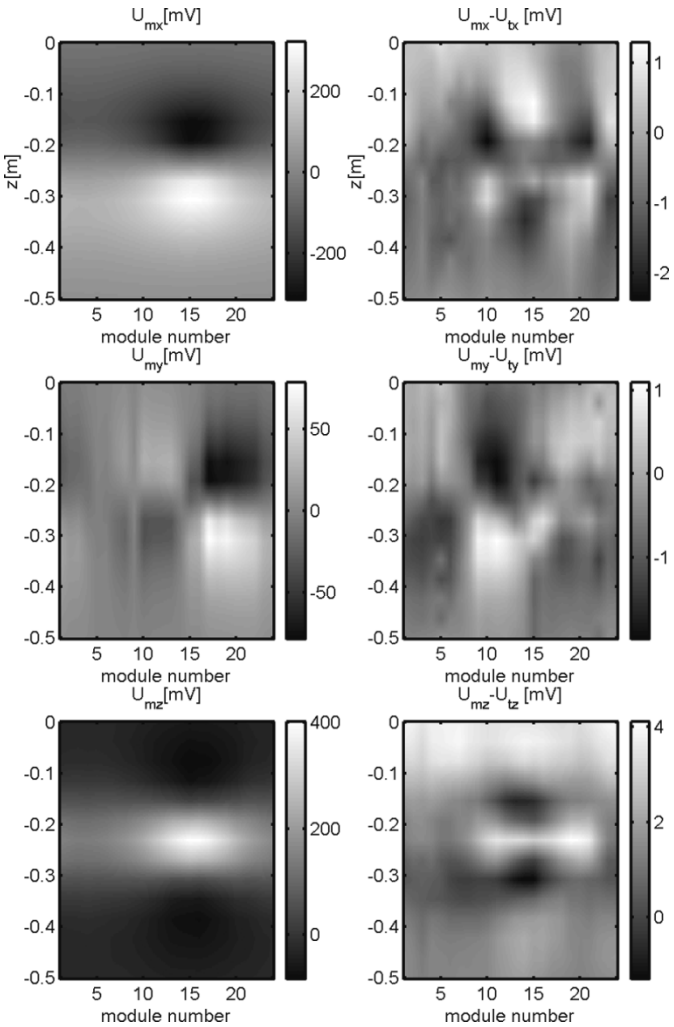

Fig. 12. Test measurements, comparison of measured and theoretical sensor signals of a coil. Measured sensor voltages U_{mx}, U_{my}, U_{mz} for the x, y, and z sensor and difference between measured and modeled values $U_{mx} - U_{tx}$, $U_{my} - U_{ty}$, and $U_{mz} - U_{tz}$ for the x, y,and z sensors. The orientation of the magnetic axes x, y, z are in relation to each module circuit board.

on the radial direction. Approximately the first half of the modules measure higher values than the second half. This behavior points to a systematic error, where some source from outside the system interferes with the measurement.

The standard deviations (noise) of the measured magnetic field are 26, 33, and 39 pT for the x, y, and z sensor and correspond well with the calculated standard deviations of the system.

Also, the effect of two not properly constructed modules (especially visible as the two vertical lines with higher amplitude in the y-axis plot) could be determined. This single-sensor y-axis chip gives rise to a more noisy behavior.

A second test was to compare the measurements of a well defined coil at a known position with the modeled sensor signals due to this coil (see Fig. 12). Both measured (U_{mx}, U_{my}, and U_{mz}) and calculated sensor voltages (U_{tx}, U_{ty}, and U_{tz}), which are proportional to the measured magnetic field, were subtracted from each other.

The maximal error in relation to the maximal value of all sensor voltages are 0.6%, 0.5%, and 1% for the x, y, and z

sensor. The rms errors are 0.20%, 0.18%, and 0.53%. The errors are probably caused by magnetic distortions due to metal in the surroundings and not by calibration errors. The z sensor shows the biggest error. Comparisons between a traditional three component fluxgate sensor (Bartington MAG-03 MSESL) with a white noise level of 3 pT/$\sqrt{\text{Hz}}$) and our sensor module show similar behavior when compared to calculated magnetic field values in a laboratory environment (see [14]).

VIII. Summary

A magnetoelectrical measurement system was designed as a tool to image electrical conductivity distributions inside cylindrical samples (0.1-m radius and 0.5-m height). The system comprises electrodes for low-frequency current injection as well as electric potential measurements and a vertically scanning torus with 24 modules to measure the three components of the magnetic field due to a current injection.

Each module consists of three orthogonal AMR sensors with a white noise level lower than 50 pT/$\sqrt{\text{Hz}}$. Since the modules are to be operated without the use of extensive magnetic shielding, field feedback circuits are implemented, negating the effect of the Earth's magnetic field on sensitivity stability. Furthermore, a lock-in amplifier with 25-Hz sine wave modulation was developed to suppress magnetic noise. In order to prevent additional magnetic fields due to current in cables a microcontroller processes, the data of a 10-s measurement cycle before sending it to a measurement computer. Calibration of the sensor modules with a triaxial Helmholtz-coil system negates the error in sensitivity and orthogonality. The measurement range of the module is $\pm$200 nT and the calibration error of the sensitivity and orthogonality is 0.1%.

Magnetic field measurements with the system without current injection show a resolution of about 35 pT and an offset error of about 200 pT, which can be corrected. Further magnetic field measurements of a well defined coil at a known position show errors of about 0.5% due to magnetic distortions of metal in the surrounding area. The current target of investigations is the reduction of this error to 0.1%.

The presented measurements and results suggest that the system is suitable for magnetoelectrical resistivity imaging studies without magnetic shielding in a typical laboratory environment.

Appendix I
Equivalent Noise Bandwidth Calculation

After the input signal from the sensor (u_m) is multiplied with the phase shifted reference signal (r_t) as part of the lock-in system, a low-pass filter is applied to the signal before it is further processed (see Fig. 7). In the MERIT system, the low-pass filter is calculated by the microcontroller as a moving average filter. In the frequency domain, the final output signal (U_a) can, therefore, be written as

$$U_a(f) = \text{FT}\left(u_m(t)r(t)\right) H_{\text{LP}}(f) \tag{11}$$

where FT denotes the Fourier transform and $H_{\text{LP}}(f)$ the moving average filter in frequency domain. This moving average filter can be written as a boxcar function with length T. The pulse response of the filter is

$$H_{\text{LP}}(t) = \frac{1}{T} \int_{-\frac{T}{2}}^{\frac{T}{2}} \delta(t)dt \tag{12}$$

and in the frequency domain

$$H_{\text{LP}}(f) = sinc(\pi f T). \tag{13}$$

The equivalent noise bandwidth is defined (see [12]) as

$$\Delta f_{\text{eq}} = \frac{\int_0^\infty |H(f)|^2 \, df}{|H(f)|^2_{\max}} = \frac{1}{2T}. \tag{14}$$

From (14), it follows that the larger the averaging time window (T), the smaller the equivalent noise bandwidth will be, and the interfering frequencies will be suppressed more. A small equivalent noise bandwidth will cause less fluctuation in the output signal [see (8)].

References

[1] B. Kulessa, U. Jaekel, A. Kemna, and H. Vereecken, "Magnetometric Resistivity (MMR) imaging of subsurface solute flow: inversion framework and laboratory tests," *J. Environ. Eng. Geophys.*, vol. 7, pp. 111–118, 2002.

[2] U. Yaramanci, A. Kemna, and H. Vereecken, "Emerging technologies and approaches in hydrogeophysics," in *Hydrogeophysics*, Y. Rubin and S. Hubbard, Eds., to be published.

[3] A. Kemna, A. Tillmann, A. Verweerd, E. Zimmermann, and H. Vereecken, "MERIT—a new magneto-electrical resistivity imaging technique: 1) modeling and tomographic reconstruction," in *Proc. 3rd World Congr. Industrial Tomography*, 2003, pp. 256–261.

[4] S. Levy, D. Adam, and Y. Bresler, "Electromagnetic impedance tomography (EMIT): a new method for impedance imaging," *IEEE Trans Med. Imag.*, vol. 21, no. 4, pp. 676–687, Apr. 2002.

[5] R. N. Edwards and M. N. Nabighian, "The Magnetometric Resistivity Method," *Electromagn. Meth. Appl. Geophys.*, vol. 2, pp. 47–105, 1991.

[6] A. Tillmann, A. Verweerd, A. Kemna, E. Zimmermann, and H. Vereecken, "Non-invasive 3D conductivity measurements with MERIT," in *Proc. SAGEEP, Environmental and Engineering Geophysical Soc.*, 2003, pp. 516–522.

[7] A. Tillmann, R. Kasteel, A. Verweerd, E. Zimmermann, A. Kemna, and H. Vereecken, "Non-invasive 3D conductivity measurements during flow experiments in columns with MERIT," in *Proc. SAGEEP, Environmental and Engineering Geophysical Soc.*, 2004, pp. 618–624.

[8] H. Hauser and M. Tondra, *Magnetic Sensors and Magnetometers*, P. Ripka, Ed. Boston, MA: Artech House, 2001, pp. 129–171.

[9] U. Dibbern, "Magnetoresistive sensors," in *Sensors*, R. Boll and K. J. Overschott, Eds. Weinheim, Germany: VCH, 1989, vol. 5, pp. 342–380.

[10] Magnetic sensors cross-axis effect, B. Pant and M. Caruso. [Online]. Available: http://www.ssec.honeywell.com/magnetic/datasheets.html

[11] S. Tumanski, *Thin Film Magnetoresistive Sensors*. Bristol, U.K.: IOP, p. 142.

[12] R. Müller, "Rauschen," in *Halbleiter-Elektronik*. Berlin, Germany: Springer Verlag, 1990, vol. 15, pp. 94–96.

[13] A brief introduction to sigma delta conversion, D. Jarman. [Online]. Available: http://www.intersil.com/support/parametric_data.asp?x=AppNote

[14] E. Zimmermann, A. Verweerd, W. Glaas, A. Tillmann, and A. Kemna, "MERIT—a new magneto-electrical resistivity imaging technique: 2) magnetic sensors and instrumentation," in *Proc. 3rd World Congr. Industrial Process Tomography*, 2003, pp. 262–267.

Egon Zimmermann received the diploma degree in communications engineering from the Fachhochschule in Aachen, Division Jülich, Germany, and the diploma degree in electrical engineering from the Fernuniversitaet, Hagen, Germany, in 1986 and 1992, respectively.

Since 1986, he has been working as an Engineer and, since 1992, as a Scientist at the Forschungszentrum Jülich GmbH, Jülich, Germany, where he developed measurement systems for temperature measurements (Johnson noise thermometry), magnetic measurements (SQUID, GMR, and AMR electronics), and imaging systems (scanning SQUID microscopy and magnetoelectrical impedance tomography). He is the Leader of the Electrical and Magnetic Measurement Group, Central Institute for Electronics (ZEL), Jülich. His current research interests include the development of imaging systems, with a focus on the measurements of low-level electrical and magnetic signals.

Arre Verweerd was born in Lekkerkerk, The Netherlands, in 1976. He received the degree in applied geophysics from the Utrecht of University, Utrecht, The Netherlands, in 2001. He is currently pursuing the Ph.D. degree at the University of Bonn, Bonn, Germany.

Currently, he is with the Agrosphere Institute (ICG-IV), Forschungszentrum Jülich GmbH, Jülich, Germany, where he is working on the development of a magnetoelectrical resistivity imaging system. His main interest lies in the area of potential field geophysics, with a focus on magnetics, electromagnetics, and resistivity applications.

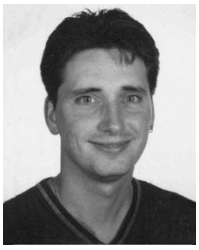

Walter Glaas was born in Jülich, Germany, 1971. He received the degree of electronic technician from the Industrie und Handelskammer Aachen ,Aachen, Germany. He is currently pursuing the German degree of Meister in electronics.

Since 1998, he has been working as a Technician at the Forschungszentrum Jülich GmbH, Jülich, with the Electrical and Magnetic Measurement Group in the Central Institute for Electronics (ZEL). His current interests include the development of hardware and software for microcontroller-based systems, with a focus on PCB design, Delphi, and C programming.

Axel Tillmann received the diploma in geophysics and the Ph.D. degree in natural sciences from the Ruhr University, Bochum, Germany, in 1997 and 2001, respectively.

From 1997 to 2001, he was a member of the scientific staff of the Geophysical Institute of the Ruhr University, where he has carried out research in the area of elastic wave propagation and electric current flow in stratified porous media. Furthermore, he worked on time-frequency analyses of dispersive waves and joint inversion theory, including the design of corresponding algorithms on parallel computers. Since 2002, he has been working as a Research Scientist at the Forschungszentrum Jülich GmbH, Jülich, Germany, where he is responsible for the development of 3-D modeling and inversion algorithms regarding MERIT. His current research interests include the further development of MERIT for geophysical and hydrological applications, especially the monitoring of fluid flow and transport processes in porous media.

Andreas Kemna received the diploma in geophysics from the University of Cologne, Cologne, Germany, and the Ph.D. degree in geophysics from the Ruhr University Bochum, Bochum, Germany, in 1995 and 2000, respectively.

From 1991 to 2000, he was with Deutsche Montan Technologie GmbH, Germany (DMT), where he became Leader of the Potential-Based Measurement Techniques Group in the Geology and Engineering Geophysics Department in 1999. In 1996, he was a Research Assistant with the Center for Research on Environmental Systems and Statistics, Lancaster University, Lancaster, U.K. In 2000, Kemna joined the Institute of Chemistry and Dynamics of the Geosphere at the Forschungszentrum Jülich GmbH, Jülich, Germany, where he is now Leader of the Noninvasive Measurement Techniques Group of the Agrosphere Institute (ICG-IV), Jülich. His main research interests include electrical and electromagnetic modeling and inversion techniques, electrical soil and rock properties, and hydrogeophysics, particularly the imaging and characterization of subsurface flow and transport.